Constraining Magnetic Dipole Dark Matter through Asteroseismology

Martim Branca

CENTRA, Departamento de Física, Instituto Superior Técnico, Universidade de Lisboa, Lisboa, Portugal

Over the last decades, dark matter has been a topic of increasing interest, especially due to our lack of knowledge about it. Several detection experiments have been developed, attempting to detect signals of its existence, even though only constraints to its fundamental properties have been obtained to date. In this work, we were able to constrain dark matter using stars. In particular, we analysed the effects of magnetic dipole dark matter in two stars younger than the Sun, KIC 8379927 and KIC 10454113. Taking advantage of stellar evolution codes, we were able to model these stars and study the impact that the captured dark matter particles have on them. Running asteroseismic tests on the stars, we managed to constrain magnetic dipole dark matter's properties, namely its mass and magnetic dipole moment. Through our analysis, we obtained competitive constraints when compared to the ones obtained by current detection experiments, limiting the magnetic moment for masses in the order of 5 GeV, where detectors are less sensitive. We proved that constraining dark matter through asteroseismology is a valid and effective method, complementing the efforts by modern detectors to identify the dark matter particle.

I. INTRODUCTION

Humanity has always been driven by the search of the unknown. This is why one of the greatest goals in the past decades and in the next to come is to detect and identify the nature of Dark Matter (DM), a nonbaryonic type of matter unlike any other seen in our universe. It has never been directly observed, although there is a good amount of indirect evidence that points towards its existence.

The most accurate determination of the energy density of dark matter in our universe comes from global fits of cosmological parameters to a wide number of observations. In particular, the most recent Wilkinson Microwave Anisotropy Probe (WMAP) results [1] show values for the cosmological parameters based on the "ΛCDM" model: a model accounting for the presence of Cold Dark Matter (CDM) on a flat universe dominated by a cosmological constant Λ. Different results for the cosmological parameters can be obtained through different combinations of observational data. In this case, we present the results obtained with the WMAP data combined with observations from the South Pole Telescope, the Atacama Cosmology Telescope, Supernova Legacy Survey's three year sample, and measurements of the baryon acoustic oscillation scale and of the Hubble constant. According to these results, only a very small part of the universe is composed by baryonic matter, corresponding to a baryon energy density of $\Omega_b = 0.04601 \pm 0.00091$, while the vast majority corresponds to dark energy, having a density of $\Omega_\Lambda = 0.7165^{+0.0093}_{-0.0094}$. Finally, the result obtained for cold dark matter shows an energy density of $\Omega_\chi = 0.2375 \pm 0.0085$.

A crucial part in the study of dark matter is of course to determine which kind of particle actually constitutes this type of matter. There are several candidates for dark matter, from which perhaps the most widely studied corresponds to Weakly Interacting Massive Particles. Also known as WIMPs, these are hypothetical particles only able to interact through gravity and the weak force, from which the most well-known and motivated type of particle is the neutralino. Neutralinos are particles that arise from supersymmetry, a greatly motivated extension to the Standard Model, although still unverified. Assuming R-parity conservation in the supersymmetric theory, the lightest of the four types of neutralinos is stable and can account for the dark matter that exists in the universe.

In fact, it can be shown that if a GeV-TeV scale particle was thermally produced and has a similar abundance to the measured density of dark matter, then the thermally averaged annihilation cross section $\langle \sigma_A v \rangle$ must be on the order of 3×10^{-26} cm^3/s [2]. On the other hand, the obtained value of $\langle \sigma_A v \rangle$ for a generic weak-scale interacting particle (such as WIMPs) is $\langle \sigma_A v \rangle \sim 3 \times 10^{-26}$ cm^3/s. This similarity is quite remarkable, and has led people to often call it as the "WIMP miracle", since this basically means that if a WIMP particle was thermally produced, it could account for the currently measured density of dark matter. This leads to a great interest and motivation in the study of WIMPs as the main component of dark matter.

Within the past decades, there have been several experiments with the objective of detecting in some way the existence of WIMPs in our universe. In particular, direct detection experiments attempt to observe nuclei recoils caused by their interaction with WIMPs via scintillation detectors. In 2010, the cumulative exposure of DAMA/NaI and DAMA/LIBRA experiments suggested the presence of dark matter based on an annual modulation obtained with 8.9σ confidence level, which was expected to exist due to the relative motion of the Earth around the Sun [3]. This became an exciting yet controversial positive result, since null results from several experiments including CDMS [4], PandaX-II [5], LUX [6], and XENON1T [7] seem to exclude the results obtained by DAMA/LIBRA, as well as other positive results from experiments such as CoGeNT [8]. V. Barger et al. [9] has suggested that certain DM particle models

could explain this inconsistency. One of the DM models suggested is Magnetic Dipole Dark Matter (MDDM), which will be the main focus of this work. XENON1T, successor of the previous experiment XENON100 [10], is the most sensitive detector to date searching for WIMPs and has set the most stringent constraints on the spin-independent WIMP-nucleon interaction cross section for WIMP masses above 10 GeV. Additionally, particle accelerators, like the Large Hadron Collider (LHC), have been trying to produce WIMPs through particle collisions and can also help us put constraints to dark matter's properties [11].

Following this introductory section, we continue with section II, in which we describe the behaviour of dark matter inside the star. We start by explaining the properties of the dark matter model we will be using, which will be magnetic dipole dark matter. We will then describe DM capture, how the number of captured DM particles inside the star changes over time, and the effect that these DM particles have on the stellar energy transport. At section III, we explain the concept of asteroseismology, together with the asteroseismic diagnostics that we will use. We will follow by providing our results, obtaining constraints for MDDM's mass and magnetic dipole moment. We will still analyse the core of dark matter particles that exists inside the stars and the effect it will have in the stellar core. Finally, at section IV, we present some conclusions on the results obtained.

II. DARK MATTER INSIDE STARS

Our whole galaxy and the stars inside it are presumed to be surrounded by a dark matter halo. Due to gravitational interaction, these DM particles will inevitably be attracted to stars, which will cause a change in the behaviour and properties of those stars. The analysis of these changes of behaviour will ultimately allow us to test the impact of DM in the star's evolution. This reveals the importance of studying DM effects in stellar interiors, which goes through how the population of DM particles N_χ changes inside a star and the way those particles will affect the energy transport mechanisms of the star. The description of capture and transport in this work follows the one taken in I. Lopes et al. [12], based on the work of Spergel and Press [13]. We will start by describing the properties of the type of dark matter we will be treating, which is magnetic dipole dark matter, followed by a description of DM capture and energy transport by the star.

A. Magnetic Dipole Dark Matter

In this work, we will consider the existence of dipole moments in dark matter. Motivated by the fact that many elementary particles have an intrinsic magnetic dipole moment but no observational evidence of a non-zero electric dipole moment (as the electron, for example), the existence of magnetic dipole dark matter is very plausible. Additionally, V. Barger et al. [9] has shown that a dark matter particle with a magnetic dipole moment could explain the discrepancies between direct detection results and successfully explain the positive results obtained by DAMA/LIBRA and CoGeNT. One should be aware that these dipole moments, if existent, must be very weak, since the coupling of dark matter with the photon is considered to be either non-existent or extremely weak. However, it is shown in I. Lopes et al. [12] that this type of matter can make a significant impact in the evolution of the star and help to effectively constrain dark matter properties, our ultimate goal.

Since we will be treating magnetic dipole dark matter, it is important to understand the properties of this type of DM. We have that the interaction of a dark matter particle χ with a magnetic dipole moment μ_χ, with an electromagnetic field $F^{\mu\nu}$ is given by [12]

$$\mathcal{L} = \frac{1}{2}\mu_\chi \bar{\chi}\sigma_{\mu\nu}F^{\mu\nu}\chi\,. \tag{1}$$

where $\sigma_{\mu\nu} = \frac{i}{2}(\gamma_\mu\gamma_\nu - \gamma_\nu\gamma_\mu)$, with γ_μ being the Dirac matrices. Additionally, this interaction vanishes for Majorana fermions, which are particles that are their own anti-particles. Therefore, MDDM particles can only consist of Dirac fermions. We are also able to determine the differential cross section for the scattering between the dark matter particle and a nucleus, via an electromagnetic interaction, which can be written as

$$\frac{d\sigma}{dE_R} = \frac{e^2\mu_\chi^2}{4\pi v_r^2}\frac{S_\chi+1}{3S_\chi}\left[Z^2\left(\frac{v^2}{E_R} - \frac{1}{2m_N} - \frac{1}{m_\chi}\right)|G_E(E_R)|^2 + \frac{S_N+1}{3S_N}\left(\frac{\mu_N}{e/(2m_p)}\right)^2\frac{m_N}{m_p^2}|G_M(E_R)|^2\right], \tag{2}$$

where $E_R = \frac{q^2}{2m_N}$ is the recoil energy for momentum transfer q, with m_N being the nucleus mass, S_χ is the DM particle spin, v_r is the incoming velocity of the DM particle in the lab. frame, Ze is the nucleus charge, m_χ is the dark matter particle mass, S_N is the nucleus spin, m_p is the proton mass, μ_N is the nucleus magnetic dipole moment, and $G_E(E_R)$ and $G_M(E_R)$, normalized to $G_{E,M}(0) = 1$, are the electric and magnetic form factors, respectively.

The relation above describes the interactions between the MDDM particles and the nuclei inside the star and will be dependent on Z, which will differ according to the different elements in the star. As we are treating solar-like stars, we know that even though there are many different elements inside the star, metals will mostly account for a very small part of the star's mass, the majority be-

ing hydrogen and helium. The amount of helium can increase to considerable values, but mostly in the core of the star, and since it has an atomic number of $Z = 2$, we can consider only the interaction of the dark matter with hydrogen, to a good approximation, as it always remains at a higher abundance than the other elements.

The total interaction cross section of MDDM with hydrogen can then be written as a sum of the spin-dependent and spin-independent cross sections [14] $\sigma_{\chi p} = \sigma^{SD}_{\chi p} + \sigma^{SI}_{\chi p}$, where

$$\sigma^{SD}_{\chi p} = \frac{\mu_\chi^2 e^2}{2\pi} \left(\frac{\mu_p}{e/(2m_p)} \right)^2 \frac{m_r^2}{m_p^2} \tag{3}$$

and

$$\sigma^{SI}_{\chi p} = \frac{\mu_\chi^2 e^2}{2\pi} \left(1 - \frac{m_r^2}{2m_p^2} - \frac{m_r^2}{m_p m_\chi} \right) , \tag{4}$$

with μ_p being the magnetic dipole moment of the proton.

B. Dark Matter Capture

In order to describe DM accumulation in stars, we must calculate the number of DM particles inside a star, which, as reviewed by Petraki and Volkas [15], changes according to the following differential equation:

$$\frac{dN_\chi(t)}{dt} = C_C + (C_S - C_E - C_{CA})\, N_\chi(t) - C_{SA}\, N_\chi^2(t) , \tag{5}$$

where C_C is the capture rate due to DM-nucleon collisions, while $C_S\, N_\chi(t)$ is the capture rate due to DM self-interaction. This happens when a DM particle enters the star and scatters with a nucleus inside the star, or with another already captured DM particle in the case of self-interaction, losing enough energy for its velocity to become smaller than the star's escape velocity, effectively becoming gravitationally bound to the star.

There can also be DM self-annihilation inside the star, which is described by the term $C_{SA}\, N_\chi^2(t)$. In this work we will assume that dark matter possesses an asymmetry, which will have a significant impact on this term. There are several models that suggest explanations for the existence of asymmetric dark matter, such as mirror dark matter [16], darkogenesis [17], and pangenesis [18]. Furthermore, by assuming a dark matter asymmetry, we can neglect C_{SA}, since the DM particles inside the star will be much more abundant than the anti-particles, hence making a bigger impact in the star's evolution. $C_{CA}\, N_\chi(t)$ accounts for the potential co-annihilation of the DM particles with nucleons, which we will neglect in this work.

Finally, C_E is the evaporation rate. DM evaporation happens when collisions between light DM particles and nuclei inside the star cause those light DM particles to escape the star's gravitational field, significantly reducing the DM impact on the stellar core. However, this effect is only relevant when $m_\chi \leqslant 4$ GeV [19], and can therefore be considered negligible for higher masses.

As such, for our work, the only non-negligible terms that will remain on the right-hand side of equation (5) will be C_C and $C_S\, N_\chi(t)$, which will indeed be the terms responsible for capture of DM by the star and will therefore maximize its impact on the star's evolution. The number of DM particles inside the star will then change according to the relation

$$N_\chi(t) = \frac{C_C}{C_S} \left(e^{C_S t} - 1 \right) , \tag{6}$$

which will grow exponentially until a geometric limit is reached where the DM self-capture saturates. This happens when all DM particles are captured when incident to the DM core with radius r_χ, which is the region inside the star where the DM distribution is concentrated. This point is reached when $\sigma_{\chi\chi} N_\chi = \pi r_\chi^2$, with $\sigma_{\chi\chi}$ being the DM self-interaction cross section, after which the DM self-capture rate will become constant and the number of DM particles in the star will start growing linearly, instead of exponentially, as can be verified by equation (5). In this work we will assume $\sigma_{\chi\chi} = 10^{-24}$ cm^2, based on the fact that the most stringent constraints of this cross section indicate that $\sigma_{\chi\chi} < 2 \times 10^{-24}$ cm^2 through Bullet Cluster observations [20, 21]. Additionally, the DM core radius $r_\chi \ll R_*$ can be described by [15, 22]

$$r_\chi = \sqrt{\frac{9 T_c}{4\pi G \rho_c m_\chi}} , \tag{7}$$

where T_c and ρ_c are the temperature and density of the stellar core, respectively.

C. Energy Transport

We now analyse the energy transport inside the star, which will be done through the description of the dark matter density and luminosity as a function of the stellar radius. There are two distinct regimes where the properties of energy transport differ from each other. These two regimes can be differentiated through the Knudsen number, K, defined by $K \equiv l_\chi / r_\chi$, where r_χ is the dark matter distribution's radius, as defined in equation (7), and l_χ is the DM particle's mean free path, given by

$$l_\chi(r) = \left[\sum_i \sigma_i n_i(r) \right]^{-1} , \tag{8}$$

with $n_i(r)$ being the local number density of the ith species of nuclei and σ_i its total interaction cross section

with the elementary particles.

In stellar regions where $l_\chi \ll r_\chi$, or equivalently $K \ll 1$, the dark matter scattering cross sections with the star's nuclei will be large, which will make collisions much more frequent, and therefore, the mean free path will be much smaller than the radius of the DM core in the star. This will result in a local energy transport predominated by conduction, causing the DM particles to be in Local Thermodynamic Equilibrium (LTE) with the star's nuclei, reason why this type of transport is often called LTE transport.

On the other hand, we also have the regime where $l_\chi \gg r_\chi$, or $K \gg 1$, often called Knudsen regime, where the scattering cross sections will be smaller and the mean free path larger, making the energy transport non-local, since two consecutive collisions will be farther apart from each other. We also know that in the star's core, the nuclei temperature is higher than the DM particles temperature, which means that collisions will cause a transfer of energy from the nuclei to the DM particles. Since this regime causes non-local transport, many of the DM particles will only give this energy back far from the star's core, which becomes an effective method of energy evacuation from the center of the star.

In both regimes, the dark matter number density $n_\chi(r)$ and the energy carried by DM scattering $L_\chi(r)$ can be explicitly calculated [23–25], effectively describing energy transport inside the star.

III. ASTEROSEISMIC DIAGNOSTICS AND DARK MATTER CONSTRAINTS

Analysing oscillating frequencies in stars throughout the universe plays a major role in this work, as we will see next. As such, we will start this chapter by describing stellar oscillations, followed by the explanation of asteroseismic diagnostics used in our analysis, including a brief description of the numerical codes used. Finally, we present the results obtained, effectively constraining magnetic dipole dark matter through asteroseismology using two different stars, while also analysing the behaviour of the dark matter cores inside the stars.

A. Asteroseismology

Over the last years, we have detected stellar oscillations in many stars, which have been incredibly useful to probe stellar interiors. The study of the propagation of these wave oscillations existent in stars, called asteroseismology, is of critical importance, since it can give valuable information about the star's internal layers, such as the sound speed profile inside the star, or the determination of stars properties, like their mass and radii [26], being able to improve previous values. Furthermore, it can also be extremely helpful in the study of dark matter [12, 27, 28]. The study of these oscillations specifically in the Sun is called helioseismology, and has led to a description of its internal layers with remarkable precision, with thousands of oscillation modes detected by the *SOHO* (Solar and Heliospheric Observatory) spacecraft [29]. Additionally, NASA's spacecraft *Kepler* [30] has also detected oscillation modes in over 500 different main-sequence solar-like stars, among a total of 20 000 oscillating stars, enabling a much better description of these stars, together with the *CoRoT* spacecraft [31] by ESA.

As such, a large number of normal oscillation frequencies $\nu_{n,l}$ of many stars has already been documented, where n is the radial order and l is the degree of the mode. Two useful diagnostics used in asteroseismology are the large separation, Δ_l, and the small separation d_{02}, which are given by:

$$\Delta_l(n) = \nu_{n,l} - \nu_{n-1,l} \tag{9}$$

$$d_{02}(n) = \nu_{n,0} - \nu_{n-1,2}\,. \tag{10}$$

Due to gravitational interaction, dark matter particles will accumulate more heavily in the star's core rather than in the outer layers. Therefore, to search for dark matter signatures it's better to use methods that are more sensitive to the star's core. Roxburgh and Vorontsov [32] concluded that the ratio of small to large separations r_{ij} would be a diagnostic much more sensitive to the star's core than the large and small separations, since it is independent of the structure of the star's outer layers. In our work, we will be using the ratio r_{02}, given by

$$r_{02}(n) = \frac{d_{02}(n)}{\Delta_1(n)}\,, \tag{11}$$

which will help us in the asteroseismic tests done next.

B. Constraining Diagnostic

The main objective of this work is to be able to constrain dark matter properties. In order to do this, we start by taking advantage of the stellar evolution code DMP2K [33], an adaptation of CESAM [34] that accounts for dark matter effects, which will compute a grid of several stellar models with varying mixing-length parameters, stellar masses and metallicities, while maintaining all measured quantities within their observational error. The mixing-length parameter α is used to describe the effects of convection in the star as explained by the mixing-length theory [35]. CESAM will evolve a star from the Zero Age Main Sequence (ZAMS), the moment when the star reaches a sufficiently high enough temperature to start having fusion reactions in its core, burning hydrogen into helium, until its present age. This evolution

will be mediated by observational parameter constraints, namely the logarithm of the surface gravity $log\, g$, the effective temperature T_{eff}, the metallicity ratio Z/X, where Z is the metals content and X the hydrogen content inside the star, and also the large frequency separation average $\langle \Delta\nu \rangle$. These models do not consider dark matter yet. Additionally, we also use ADIPLS [36], an oscillation frequencies and separations computing code, which will compute the normal oscillation frequencies for each of the stellar models obtained, allowing us to determine which stellar model is the closest to reality, making it our benchmark model.

Our asteroseismic analysis will be based on the statistical quantity $\chi^2_{r_{02}}$, defined by

$$\chi^2_{r_{02}} = \sum_n \left(\frac{r_{02}^{obs}(n) - r_{02}^{mod}(n)}{\sigma_{r_{02}^{obs}}(n)} \right)^2 , \tag{12}$$

where $\sigma_{r_{02}^{obs}}$ is the observational error of r_{02}^{obs}, already described in equation (11), which, as already explained, is a particularly useful diagnostic for the presence of DM in a star, since it is especially sensitive to the stellar core, where DM effects are more significant. This quantity represents the sum over the different modes of the error between the observed r_{02} ratio values and the modelled ones. By running this diagnostic through a certain DM parameter space within our stellar benchmark model, we will be able to exclude DM models that cause an incompatibility between our models and reality to a certain confidence level, effectively obtaining constraints on DM properties, as we will see next.

C. Results

In this work, two stars were analysed: KIC 8379927 and KIC 10454113, both observed by the *Kepler* spacecraft (KIC meaning *Kepler* Input Catalog). Each of these stars is slightly more massive than the Sun, showing a high precision in the determination of both the observational parameters and the detected oscillation modes. A great number of oscillation frequency modes has been observed in either star, presented in T. Appourchaux et al. [37], which is important in order to obtain realistic values of the asteroseismic diagnostics. In table I we show the observational constraints chosen for the models of both stars analysed in this work [38–41]. The benchmark models are shown in table II. Additionally, based on other works studying the DM impact on the Sun or solar-like stars [12, 27, 33], we show the numerical values for parameters used in the computation of DM capture in table III.

1. KIC 8379927 Star

From table II, we can see that the optimal model obtained for the star KIC 8379927 presents a mass of $M = 1.12\, M_\odot$, an age of $\tau = 1.77$ Gyr and a radius of $R = 1.12\, R_\odot$, being more massive and bigger in size than the Sun, while also being a much younger star, since the Sun has an age of $\tau = 4.57$ Gyr. Furthermore, this star is a good subject to run asteroseismic tests, considering that it possesses 11 distinct measured values of the r_{02} ratio, compared to the Sun's 17 observable ones.

We can now run the $\chi^2_{r_{02}}$ diagnostic through the MDDM-influenced stellar models with DM masses between 5 GeV $\leqslant m_\chi \leqslant$ 15 GeV and DM magnetic dipole moments between 10^{-17} e $\cdot$ cm $\leqslant \mu_\chi \leqslant 2 \times 10^{-15}$ e $\cdot$ cm. Calculating $\chi^2_{r_{02}}$ for each of the models, we were able to obtain the contour plot for KIC 8379927 shown in figure 1 (left).

Our $\chi^2_{r_{02}}$ analysis points to the exclusion of MDDM particles with low masses and magnetic dipole moment surrounding $\mu_\chi \simeq 10^{-16}$ e $\cdot$ cm, since there is a large disagreement between our modelled results and measured data in this region. This incompatibility between models and observational data allows certain MDDM parameters to be excluded up to a determined certainty. In particular, for an MDDM particle mass of $m_\chi \simeq 5$ GeV, we can exclude candidates with a magnetic dipole moment within 3.5×10^{-17} e $\cdot$ cm $\leqslant \mu_\chi \leqslant 3.9 \times 10^{-16}$ e $\cdot$ cm with a 95% confidence level.

Additionally, we can also perform the same $\chi^2_{r_{02}}$ tests as the ones done in figure 1 but without considering the effect of DM self-interaction in the capture of DM by the star. This effect contributes to the capture of DM particles as can be seen by equation (5), and as such, neglecting this term is expected to result in a lower DM impact in the star. However, for our case, by observing figure 2 (left), we can verify that no relevant difference is seen in the constraints when compared to the case considering DM self-interaction, shown in figure 1 (left). This may be explained by the fact that this is a rather young star, with less than half the age of the Sun, and hasn't been able to capture a large enough amount of dark matter particles in its short lifespan. Since the capture rate due to DM self-interaction is proportional to the number of DM particles inside the star, which grows over time according to equation (6), we can see the possible reason why it seems to be negligible at this age.

Although the currently standard value for the local dark matter density used in the literature is $\rho_\chi = 0.38$ GeV/cm^3, S. Garbari et al. [42] suggests a value of $\rho_\chi = 0.85^{+0.57}_{-0.50}$ GeV/cm^3, based on the kinematics of K dwarf stars. Therefore, we tested our models (considering DM self-interaction) setting the local dark matter density value to $\rho_\chi = 0.85$ GeV/cm^3 instead of the value used in the previous tests $\rho_\chi = 0.38$ GeV/cm^3. Increasing the dark matter density will cause stars to capture a higher number of DM particles, increasing their impact on the star. We present the obtained results in figure 2

Star	$log\, g\ \left(\mathrm{cm/s^2}\right)$	T_{eff} (K)	Z/X	$\langle\Delta\nu\rangle$ (μHz)
KIC 8379927 (A)	4.5 ± 0.4	6050 ± 250	0.020 ± 0.010	120 ± 5
KIC 10454113 (B)	4.3 ± 0.2	6200 ± 200	0.026 ± 0.006	105 ± 4

TABLE I. Input observational parameters for KIC 8379927 and KIC 10454113 [38–41], where $log\, g$ is the logarithm of the surface gravity, T_{eff} is the effective temperature, Z/X is the metallicity ratio, and $\langle\Delta\nu\rangle$ is the large frequency separation average.

Star	$M\ (M_\odot)$	Z	α	τ (Gyr)	$R\ (R_\odot)$	T_{eff} (K)	$L\ (L_\odot)$	Z/X	$log\, g\ \left(\mathrm{cm/s^2}\right)$	$\langle\Delta\nu\rangle$ (μHz)
A	1.12	0.0180	1.80	1.77	1.12	6157	1.62	0.0236	4.39	120.7
B	1.19	0.0180	2.00	1.96	1.23	6399	2.29	0.0221	4.33	107.7

TABLE II. Stellar parameters obtained from the benchmark models of stars KIC 8379927 (A) and KIC 10454113 (B), where $M\ (M_\odot)$ is the stellar mass related to the solar mass, Z is the metallicity, α is the mixing-length parameter, τ is the age of the star, $R\ (R_\odot)$ is the stellar radius related to the solar radius, and $L\ (L_\odot)$ is the stellar luminosity related to the solar luminosity.

$\rho_\chi\ \left(\mathrm{GeV/cm^3}\right)$	v_* (km/s)	$\overline{v_\chi}$ (km/s)	$v_{esc}\,(R_*)$ (km/s)	$\sigma_{\chi\chi}\ \left(\mathrm{cm^2}\right)$
0.38	220	270	618	10^{-24}

TABLE III. Parameters used in the computation of DM capture, where ρ_χ is the DM halo density, v_* is the stellar velocity, $\overline{v_\chi}$ is the DM velocity dispersion, $v_{esc}\,(R_*)$ is the escape velocity of the star, and $\sigma_{\chi\chi}$ is the DM self-interaction cross section.

(right), showing the exclusion of $m_\chi \simeq 5$ MDDM particles with magnetic moment between $2.7 \times 10^{-17}\ \mathrm{e \cdot cm} \leqslant \mu_\chi \leqslant 5.8 \times 10^{-16}\ \mathrm{e \cdot cm}$ with 95% CL. As expected, when compared to figure 1 (left), we verify that stronger constraints were obtained with this higher value of local dark matter density.

2. *KIC 10454113 Star*

On the other hand, the obtained benchmark model for KIC 10454113 shows a mass of $M = 1.19\, M_\odot$, an age of $\tau = 1.96$ Gyr and a radius of $R = 1.23\, R_\odot$. We see that this star is slightly more massive, bigger in size and older than KIC 8379927, while also having a substantial amount of 13 measured r_{02} ratios.

Performing the $\chi^2_{r_{02}}$ test for the star KIC 10454113, we can observe by figure 1 (right) that for MDDM masses of $m_\chi \simeq 5$ GeV, it allows the exclusion of models with magnetic dipole moment between $2.9 \times 10^{-17}\ \mathrm{e \cdot cm} \leqslant \mu_\chi \leqslant 5.9 \times 10^{-16}\ \mathrm{e \cdot cm}$ with a 95% CL.

Even though KIC 10454113 yields lower values of $\chi^2_{r_{02}}$ below the exclusion lines, we see that not only does it produce stronger constraints on MDDM but it also has higher values of $\chi^2_{r_{02}}$ in the rest of the parameter space, which evidences an overall greater DM impact in the evolution of this star. This effect can be explained due to the fact that this star is older than KIC 8379927, and since DM capture will produce a cumulative effect over time, older stars will experience a stronger DM impact. Indeed, this star does provide stronger constraints than KIC 8379927, both in terms of magnetic dipole moment as in DM mass. We see that at 95% CL, constraints can be obtained up to nearly $m_\chi \simeq 8.5$ GeV, whereas in KIC 8379927 these can only be observed up until $m_\chi \simeq 7$ GeV.

Similarly to what was done with KIC 8379927, we tested our $\chi^2_{r_{02}}$ analysis without the effect of DM self-interaction for KIC 10454113, presented in figure 3 (left). When comparing to 1 (right), we can see that, although a small change in the 99% CL constraint can be observed, there are still no major differences. Again, this may be caused by the fact that, while being a slightly older star than KIC 8379927, it still is a young star, making the self-interaction term nearly negligible.

Increasing the local DM density to $\rho_\chi = 0.85\ \mathrm{GeV/cm^3}$, we also obtained stronger constraints for KIC 10454113, comparing to the previous case shown in figure 1 (right), where $\rho_\chi = 0.38\ \mathrm{GeV/cm^3}$. Indeed, by observing the $\chi^2_{r_{02}}$ diagnostic test in figure 3 (right), we see that we can exclude MDDM particles with $m_\chi \simeq 5$ GeV and magnetic moments within $2.2 \times 10^{-17}\ \mathrm{e \cdot cm} \leqslant \mu_\chi \leqslant 8.3 \times 10^{-16}\ \mathrm{e \cdot cm}$ with 95% CL.

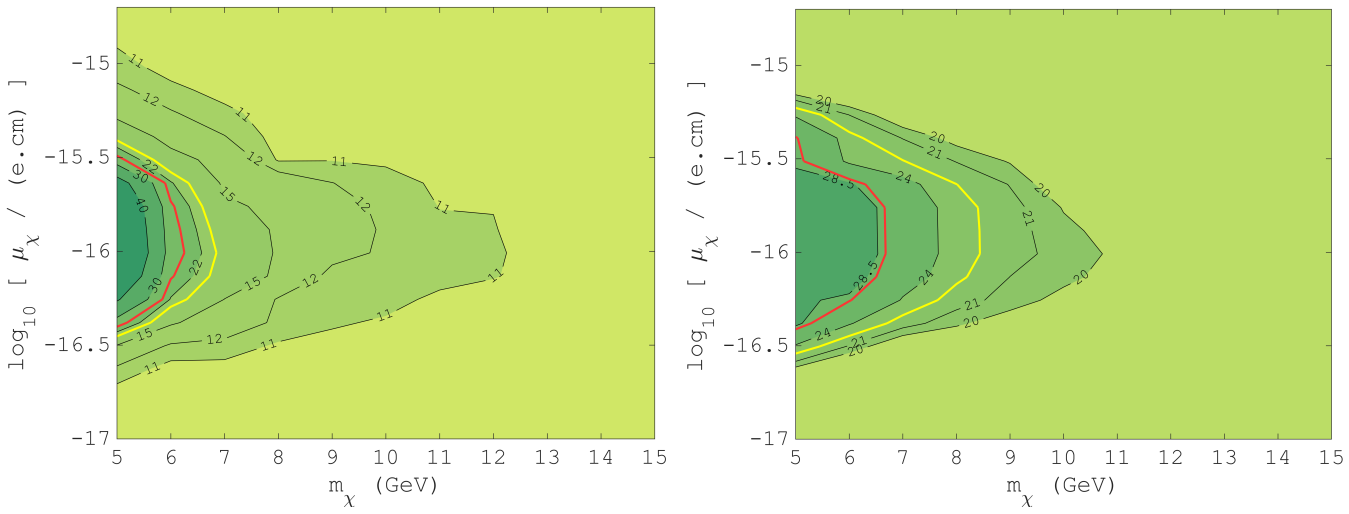

FIG. 1. Constraints on MDDM for the stars KIC 8379927 (left) and KIC 10454113 (right), with the $\chi^2_{r_{02}}$ diagnostic, showing the 95% (yellow) and 99% (red) confidence level lines (with 11 and 13 degrees of freedom for KIC 8379927 and KIC 10454113, respectively).

3. *Dark Matter Core*

As we have seen, the DM particles trapped by a star will be concentrated inside the stellar core. The distribution of such DM particles will have a certain radius r_χ, given by equation (7). This DM core radius is inversely proportional to the square root of the DM particle's mass, and as such, we are expecting the size of the DM core to increase as the MDDM particle's mass decreases. Additionally, a dark matter core inside the stellar centre provides an additional mechanism for transferring energy from the stellar core to the outer layers of the star, effectively being able to decrease the temperature in the DM core's region. In order to observe the changes that the DM particle's properties cause in the DM core's behaviour, we calculated the DM distribution's radius r_χ and the DM core's temperature T_χ for our MDDM parameter space, obtaining the contour plots shown in figure 4 for KIC 8379927 and figure 5 for KIC 10454113.

From these plots, one can verify that, as expected, the radius of the DM core does increase with decreasing DM masses. As seen by figure 4, for KIC 8379927, with MDDM particles of $m_\chi \simeq 6.5$ GeV and $\mu_\chi \simeq 10^{-16}$ e·cm, the radius of the DM core would reach $\sim 4.4\%$ of the total stellar radius. On the other hand, as for the temperature of the DM core, a similar behaviour to the $\chi^2_{r_{02}}$ analysis plot presented in figure 1 can be seen. This shows the link between DM impact and a lower core temperature, as one would expect. In particular, for KIC 10454113, with MDDM particles of $m_\chi \simeq 5.5$ GeV and $\mu_\chi \simeq 10^{-16}$ e·cm, the DM core can reach temperatures of $T_\chi \simeq 1.59 \times 10^7$ K, down from the benchmark's model (no DM influence) stellar core temperature of $T_\chi = 1.81 \times 10^7$ K. We can therefore see how effective DM can be in lowering the core's temperature and the impact it can have in the stellar structure.

IV. CONCLUSIONS

In this work we analysed the effect that magnetic dipole dark matter can have in the evolution and behaviour of solar-like stars. We started by providing the theoretical background related to MDDM and its capture and energy transport inside the star. Afterwards, by running the stellar evolution code CESAM, we modelled two stars up to their current ages, based on measured observational parameters. We then were able to calculate the statistical quantity $\chi^2_{r_{02}}$, defined by equation (12), which allowed us to constrain MDDM properties.

Our asteroseismic analysis based on this $\chi^2_{r_{02}}$ parameter presented in figure 1 shows an improvement on the 95% CL constraints of the magnetic dipole moment of $\sim 17\%$ on the lower boundary and $\sim 51\%$ on the upper boundary from KIC 8379927 to KIC 10454113 at $m_\chi \simeq 5$ GeV. The fact that KIC 10454113 provides stronger constraints can be explained by the fact that it is an older star, allowing DM to accumulate in its core for a longer period of time and leaving a larger signature. Additionally, for KIC 10454113, with $m_\chi \simeq 10$ GeV, we can exclude MDDM particles with a lower boundary of $\mu_\chi \geqslant 6.0 \times 10^{-17}$ e · cm with a 90% CL, improving the 90% CL constraints put by the LHC of $\mu_\chi \gtrsim 10^{-15}$ e·cm, using the mono-jet events plus missing transverse energy, and also the constraints put by the Large Electron-Positron Collider (LEP) of $\mu_\chi \gtrsim 10^{-16}$ e · cm, using the mono-photon plus missing transverse energy events [43]. E. Del Nobile et al. [44] shows that all the experimental results are compatible with an MDDM particle of $m_\chi \simeq 10$ GeV and $\mu_\chi \simeq 1.5 \times 10^{-18}$ e · cm. We see that these results do not get conflicted by the constraints provided in this work. This procedure provided us with a weaker constraint than the one obtained in the helioseismologic analysis carried out by I. Lopes et al. [12], in

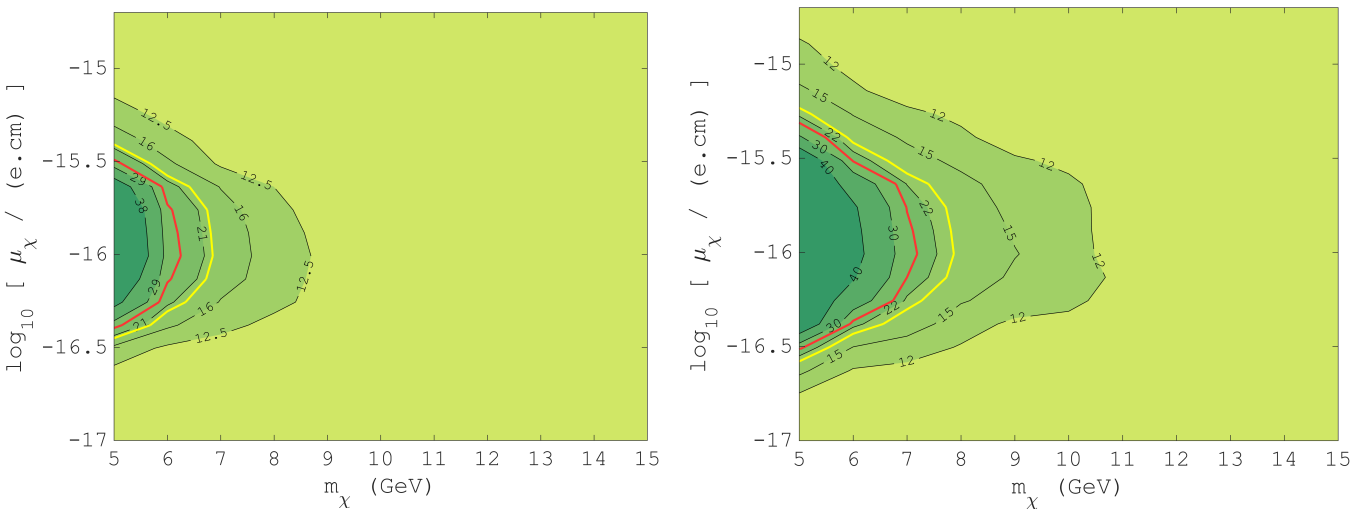

FIG. 2. Constraints on MDDM with no DM self-capture interaction (left) and with a local dark matter density of $\rho_\chi = 0.85$ GeV/cm^3 (considering DM self-interaction) (right), for the star KIC 8379927, with the $\chi^2_{r_{02}}$ diagnostic, showing the 95% (yellow) and 99% (red) CL lines (with 11 degrees of freedom).

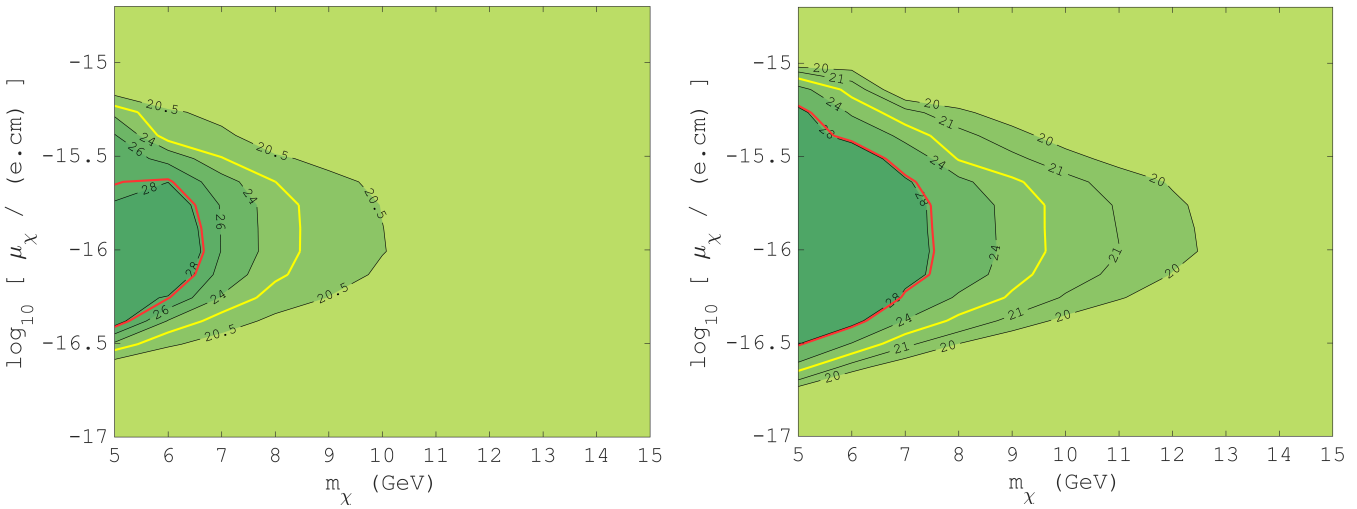

FIG. 3. Constraints on MDDM with no DM self-capture interaction (left) and with a local dark matter density of $\rho_\chi = 0.85$ GeV/cm^3 (considering DM self-interaction) (right), for the star KIC 10454113, with the $\chi^2_{r_{02}}$ diagnostic, showing the 95% (yellow) and 99% (red) CL lines (with 13 degrees of freedom).

which we can exclude particles with $m_\chi \simeq 10$ GeV and $\mu_\chi \geqslant 1.6 \times 10^{-17}$ e $\cdot$ cm. This is, however, somewhat expected at the moment, since not only does the Sun have a significant number of measured r_{02} ratios, but it also has observational data measured with a remarkably high precision. Our analysis provides competitive and independent results using the studied stars, in different evolutionary stages than the Sun, showcasing its utility and potential growth in precision within the next decades.

We have also concluded that DM self-interaction capture rate seems to be negligible for our stars. By comparison between models with DM self-interaction, in figure 1, and without it, in figure 2 and 3 (left), we can see that there are no relevant differences between the correspondent constraints. As explained before, this may happen due to the young age of our stars, as the effect is expected to become noticeable in older stars.

The effect of the local dark matter density on the DM impact inside the star was also analysed, shown in figures 2 and 3 (right). For KIC 10454113, we noticed an improvement on the 95% CL constraints of the magnetic dipole moment of $\sim 24\%$ on the lower boundary and $\sim 41\%$ on the upper boundary from models with $\rho_\chi = 0.38$ GeV/cm^3 to models with $\rho_\chi = 0.85$ GeV/cm^3, at $m_\chi \simeq 5$ GeV. We also see that, for KIC 10454113, we can only obtain 95% CL constraints up to DM masses of nearly $m_\chi \simeq 8.5$ GeV with the lower DM density, while models with the increased density allow for constraints

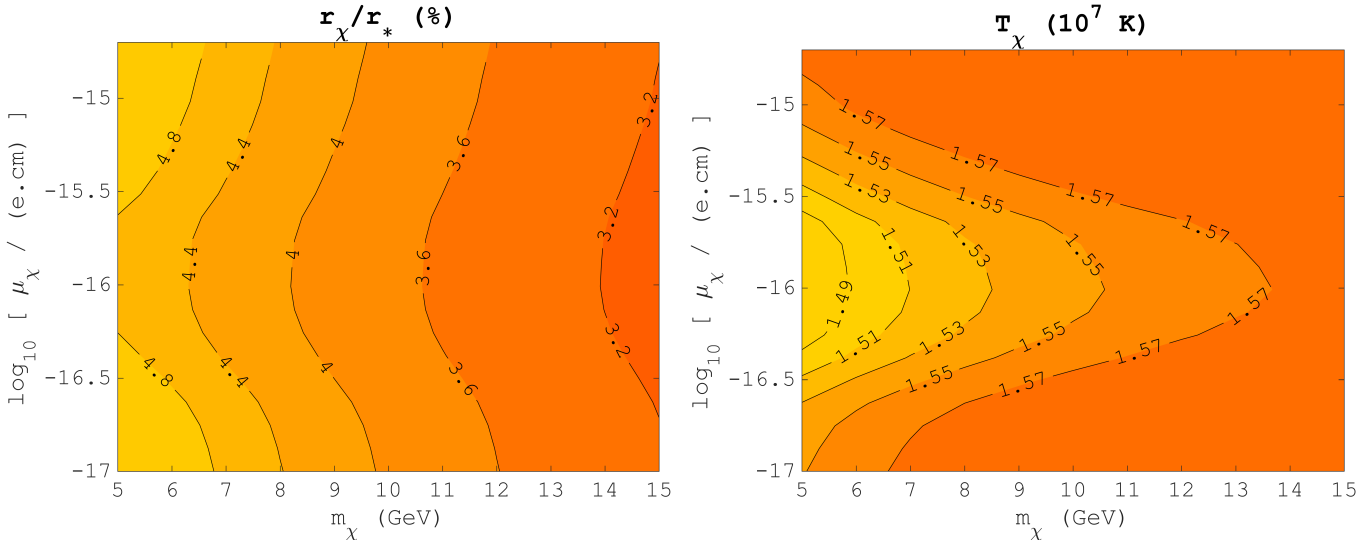

FIG. 4. Radius of the DM core related to the stellar radius (left) and DM core's temperature (right) in function of the MDDM parameter space for KIC 8379927.

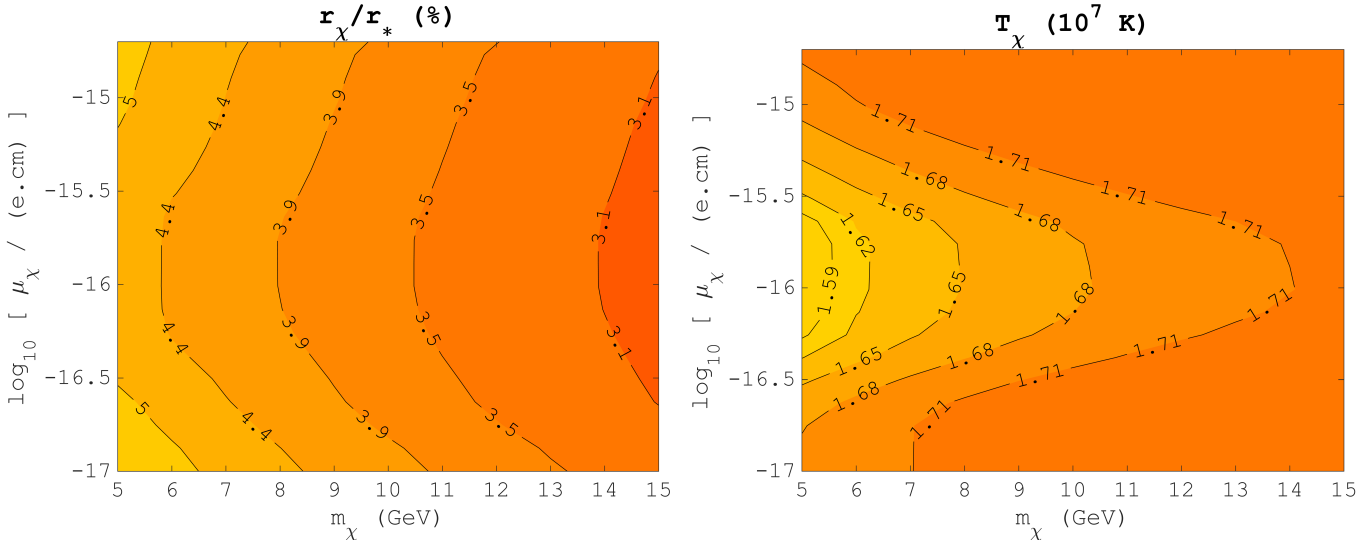

FIG. 5. Radius of the DM core related to the stellar radius (left) and DM core's temperature (right) in function of the MDDM parameter space for KIC 10454113.

up to almost $m_\chi \simeq 10$ GeV. From these results we can verify that, as expected, the local DM density can have significant effects on the DM impact in a star.

Finally, we analysed the DM core, a region inside the star where the captured DM particles will be concentrated. We observed that, as expected from equation (7), the radius of the DM core increases with decreasing DM particle masses, shown in figures 4 and 5 (left). On the other hand, analysing the temperature of the DM core, we can see that it decreases with decreasing DM particle masses, presented in figures 4 and 5 (right). This is to be expected since, as already explained, dark matter will be able to transfer energy from the stellar core to different regions of the star, and as such, a higher DM impact will be linked to a lower core temperature, which is what we can observe in the lower mass regions. In fact, for KIC 10454113, with MDDM particles of $m_\chi \simeq 5.5$ GeV and $\mu_\chi \simeq 10^{-16}$ e·cm, we see a core temperature reduction of $\sim 12\%$ from the benchmark model, due to the presence of dark matter, highlighting the potentially significant effects that DM can have in stellar cores.

In the future, asteroseismology will continue evolving as more complex stellar models regarding the evolution and dark matter effects inside the star are developed and as more precise observational data is collected through increasingly better spacecrafts. A possible improvement to the work developed here could be to account for the evaporation effects that become relevant for masses $m_\chi \leqslant 4$ GeV, enabling the study and constraining of lower masses. Another improvement would

be accounting for the interaction of dark matter with other elements in the star, instead of only hydrogen, in order to obtain more realistic and precise results. There are also two spacecrafts to be deployed in the upcoming years, which represent an important step in asteroseismology. These are the Transiting Exoplanet Survey Satellite (*TESS*), from NASA and planned to be launched in March 2018, and Planetary Transits and Oscillations of stars (*PLATO*), from ESA and planned to be launched in 2026. Both these spacecrafts will be able to measure numerous stellar oscillation mode frequencies with an impressive level of precision, in our case allowing us to study and constrain dark matter inside stars much more precisely.

As a final note, we have shown that asteroseismology can be an alternative and unique method to study dark matter and provide strong and competitive constraints to it, representing one step forward in the the search for the elusive dark matter particle.

ACKNOWLEDGMENTS

The author thanks Prof. Ilídio Lopes and CENTRA for providing the necessary tools and support in order to complete this work.

[1] G. Hinshaw et al., The Astrophysical Journal Supplement Series **208** (2013) 19.
[2] D. Hooper, arXiv preprint [arXiv:0901.4090] (2009).
[3] R. Bernabei et al., The European Physical Journal C **67** (2010) 39.
[4] R. Agnese et al., Physical Review D **88** (2013) 031104.
[5] A. Tan et al., Physical Review Letters **117** (2016) 121303.
[6] D. Akerib et al., Physical Review Letters **118** (2017) 021303.
[7] E. Aprile et al., arXiv preprint [arXiv:1705.06655] (2017).
[8] C. Aalseth et al., Physical Review D **88** (2013) 012002.
[9] V. Barger, W. Y. Keung and D. Marfatia, Physics Letters B **696** (2011) 74.
[10] E. Aprile et al., Physical Review D **94** (2016) 122001.
[11] V. Khachatryan et al., The European Physical Journal C **75** (2015) 235.
[12] I. Lopes, K. Kadota and J. Silk, The Astrophysical Journal Letters **780** (2013) L15.
[13] D. Spergel and W. H. Press, The Astrophysical Journal **294** (1985) 663.
[14] V. Barger et al., Physics Letters B **717** (2012) 219.
[15] K. Petraki and R. Volkas, International Journal of Modern Physics A **28** (2013) 1330028.
[16] Z. Berezhiani, The European Physical Journal Special Topics **163** (2008) 271.
[17] J. Shelton and K. Zurek, Physical Review D **82** (2010) 123512.
[18] B. Harling, K. Petraki and R. Volkas, Journal of Cosmology and Astroparticle Physics **2012** (2012) 021.
[19] A. Gould, The Astrophysical Journal **356** (1990) 302.
[20] T. Güver et al., Journal of Cosmology and Astroparticle Physics **2014** (2014) 013.
[21] M. Markevitch et al., The Astrophysical Journal **606** (2004) 819.
[22] K. Griest and D. Seckel, Nuclear Physics B **283** (1987) 681.
[23] B. Geytenbeek et al., Journal of Cosmology and Astroparticle Physics **2017** (2017) 029.
[24] A. Gould and G. Raffelt, The Astrophysical Journal **352** (1990) 654.
[25] P. Scott, M. Fairbairn and J. Edsjö, Monthly Notices of the Royal Astronomical Society **394** (2009) 82.
[26] V. Aguirre et al., Monthly Notices of the Royal Astronomical Society **452** (2015) 2127.
[27] J. Casanellas and I. Lopes, The Astrophysical Journal Letters **765** (2013) L21.
[28] A. Martins, I. Lopes and J. Casanellas, Physical Review D **95** (2017) 023507.
[29] V. Domingo, B. Fleck and A. Poland, Solar Physics **162** (1995) 1.
[30] R. Gilliland et al., Publications of the Astronomical Society of the Pacific **122** (2010) 131.
[31] B. Mosser et al., Astronomy & Astrophysics **532** (2011) A86.
[32] I. Roxburgh and S. Vorontsov, Astronomy & Astrophysics **411** (2003) 215.
[33] I. Lopes, J. Casanellas and D. Eugénio, Physical Review D **83** (2011) 063521.
[34] P. Morel and Y. Lebreton, Astrophysics and Space Science **316** (2008) 61.
[35] E. Böhm-Vitense, Zeitschrift fur Astrophysik **46** (1958) 108.
[36] J. Christensen-Dalsgaard, Astrophysics and Space Science **316** (2008) 113.
[37] T. Appourchaux et al., Astronomy & Astrophysics **543** (2012) A54.
[38] C. Karoff et al., Monthly Notices of the Royal Astronomical Society **433** (2013) 3227.
[39] J. Molenda-Żakowicz et al., Monthly Notices of the Royal Astronomical Society **434** (2013) 1422.
[40] S. Mathur et al., The Astrophysical Journal **749** (2012) 152.
[41] H. Bruntt et al., Monthly Notices of the Royal Astronomical Society **423** (2012) 122.
[42] S. Garbari et al., Monthly Notices of the Royal Astronomical Society **425** (2012) 1445.
[43] J. F. Fortin and T. Tait, Physical Review D **85** (2012) 063506.
[44] E. Del Nobile et al., Journal of Cosmology and Astroparticle Physics **2012** (2012) 010.